High-resolution infrared study of vinyl acetylene: the ν_{13} (214 cm^{-1}) and ν_{18} (304 cm^{-1}) fundamentals

Christian P. Endres[a,*], Georg Ch. Mellau[b], Michael E. Harding[c], Marie-Aline Martin-Drumel[d], Holger Lichau[e,1], Sven Thorwirth[e]

[a]*Max-Planck-Institut für extraterrestrische Physik, 85748 Garching, Germany*
[b]*Physikalisch-Chemisches Institut, Justus-Liebig-Universität Gießen, Heinrich-Buff-Ring 17, 35392 Gießen, Germany*
[c]*Institut für Nanotechnologie, Karlsruher Institut für Technologie (KIT), Campus Nord, Postfach 3640, 76021 Karlsruhe, Germany*
[d]*Université Paris-Saclay, CNRS, Institut des Sciences Moléculaires d'Orsay, 91405 Orsay, France*
[e]*I. Physikalisches Institut, Universität zu Köln, Zülpicher Straße 77, 50937 Köln, Germany*

Abstract

The high resolution vibrational spectrum of vinyl acetylene (C_2H_3CCH) has been investigated in the far infrared region from 180 to 360 cm^{-1} using the Bruker IFS 120 HR spectrometer at Justus-Liebig-Universität, Gießen, Germany. The two energetically lowest vibrational fundamentals ν_{13} and ν_{18} at 214 cm^{-1} and 304 cm^{-1}, respectively, were measured at a resolution of 0.0016 cm^{-1}. In addition to the fundamental modes, several hot bands originating from either ν_{13} or ν_{18} were observed and analyzed. The spectroscopic analysis was supported by high-level quantum chemical coupled-cluster calculations.

In addition to the infrared study, so far unpublished millimeter-wave vibrational satellites that were measured in the course of an earlier study of the pure rotational spectrum of vinyl acetylene in its ground vibrational state (Thorwirth and Lichau, Astron. Astrophys. 398, L11, 2003) were added to the data set and are reported here for the first time.

Keywords: Vinyl acetylene, Butenyne, Far-IR rotation-vibration, Quantum chemical calculations, FTIR

1. Introduction

Vinyl acetylene (but-1-en-3-yne, $H_2C=CH-C\equiv CH$, hereafter VA) is the simplest enyne, a pure hydrocarbon molecule of relevance for astrochemistry [1, 2] and as such has triggered a number of spectroscopic investigations in the past. The ground state a-type pure rotational spectrum of this moderately polar molecule ($\mu_a = 0.4$ D, $\mu_b \approx 0$ D [cf. Refs. 3–5]) has been studied from the microwave into to the submillimeter regime reaching frequencies as high as 790 GHz [4, 6–10]. Vibrational satellites from the energetically low-lying first and even multiply

excited modes ν_{13} (C$-$C$\equiv$C in-plane (ip) bending, a') and ν_{18} (C$-$C$\equiv$C out-of-plane (oop) bending, a'') in the parent and the $H_2C=CH-C\equiv CD$ species were also reported early on [7, 8] but so far have been restricted to the microwave region.

Over the years, some insight into the infrared (IR) spectrum of VA has also been gained [2, 8]. Probably the most comprehensive study dates back to 1980 when Tørneng et al. [8] observed IR and Raman spectra of VA as a solid, a neat liquid, and in the gas phase in the 100 to 5000 cm^{-1} range and identified the vibrational fundamentals along with a plethora of overtones and combination modes. However, the corresponding gas-phase study was performed at moderate resolution only (≥ 0.5 cm^{-1}) and hence did not permit analysis of the finer rotation-vibration details. So far, there appears to be only one observation of a fully resolved rotation-vibration spectrum of VA, covering a few cm^{-1} within the ν_1 (ethynyl C$-$H stretching)

---

band around $3325\,\text{cm}^{-1}$ and taken during a study of jet-cooled propargyl radical [11]. However, neither detailed spectroscopic analysis of the rotation-vibration transitions nor experimental frequencies was presented there.

In the present investigation, the high-resolution far-infrared spectrum of VA has now been observed from 180 to $360\,\text{cm}^{-1}$ encompassing the two energetically lowest vibrational fundamentals, ν_{13} and ν_{18}, located at $214\,\text{cm}^{-1}$ and $304\,\text{cm}^{-1}$, respectively. Close inspection of the spectrum obtained did not only reveal the presence of the vibrational fundamentals but also of hot bands. In addition, the new IR dataset has been complemented with millimeter-wave vibrational satellites of VA in the $v_{13} = 1$ and $v_{18} = 1$ states. Those satellites were identified in spectra covering the $3\,\text{mm}$ range (80 to 119 GHz) taken during a study of the ground vibrational state spectrum [4] and are reported here for the first time. The experimental study is further supported by high-level quantum-chemical calculations of the molecular force field performed at at the coupled-cluster singles and doubles model augmented by a perturbative correction for triple excitations (CCSD(T)) level of theory.

2. Experiment

The sample of VA used in the present studies was synthesized by di-dehydrochlorination of 1,4-dichloro-2-butene according to the recipe given by Tørneng et al. [8] and kept under liquid nitrogen for storage.

2.1. Far-IR measurements

The high-resolution far-infrared (FIR) absorption spectrum of VA was studied from 180 to $360\,\text{cm}^{-1}$ using the Bruker IFS 120 HR spectrometer at Justus-Liebig-Universität Gießen, Germany. The spectrum shown in Fig. 1 was recorded at a temperature of $-83\,°C$ using a temperature controlled absorption cell (mainly designed for intensity measurements) described in detail in Schermaul et al. [12]. The 302 cm long cell is surrounded by a sand bath and a liquid nitrogen conducting tube system. Computer-controlled cooling bursts of liquid nitrogen are generated to cool the sand bath. A set of 16 independent heating elements are used to stabilize the cell temperature to a selected value in a computer-controlled closed loop. Once the sand temperature has reached the selected value, the system is extremely robust against the cooling effect of the individual bursts and there are no super-cooled spots on the cell surface.

Two high-resolution spectra were recorded at a resolution (1/MOPD) of 0.00188 cm^{-1} using an iris aperture diameter of 2.5 mm (focal length of the collimator mirror f_{col}=41.8 cm), the mercury lamp of the IFS120 as FIR source, and a liquid He cooled Si-Bolometer. The first spectrum consists of 286 co-averaged scans recorded at 297.8(3) K (RT) and a sample pressure of 2.0(1) mbar; the second spectrum results from the averaging of 199 scans at 190.2(10) K $(-83\,°C)$ and 0.70(10) mbar (Fig. 2). The frequency axis of both spectra were calibrated with residual water lines [13].

Even though the natural (Doppler) full width at half maximum (FWHM) of the lines of VA at room temperature and -83 °C $(0.00055\,\text{cm}^{-1}$ and $0.00044\,\text{cm}^{-1}$, respectively, at $318.5\,\text{cm}^{-1})$ is lower than that resulting from the limited instrumental resolution $(0.0013\,\text{cm}^{-1}$ ideally and $0.0016\,\text{cm}^{-1}$ observed experimentally due to the apodization effect of the aperture and pressure broadening), recording the VA spectrum at -83 °C allows to better resolve spectral features that slightly overlap at room temperature, as illustrated in Fig. 2. We see that for our instrument, the apparent FWHM in the FIR region is not sensitive to the decrease of the Doppler width when the cooling of the molecular gas is achieved by simply cooling the sample cell down to a temperature that still ensures an appreciable amount of sample vapor pressure. The slight change in apparent resolution is rather due to the lower pressure required to obtain the nearly identical cold spectrum (in terms of absorbance) and the simplification of the spectrum due to the reduction of the molecular partition function. For that reason, the following analysis has been performed on the cold spectrum only. Another positive aspect of the cooling is that it significantly reduces spectral interference with lines of residual water vapor in the absorption cell.

2.2. Millimeter-wave measurements

Millimeter-wave vibrational satellites from the $v_{13} = 1$ and $v_{18} = 1$ states were measured at room temperature and obtained in the course of the study of ground-state millimeter-wave spectrum reported earlier [4]. They are reported here for the first time. Measurements were performed with a commercial spectrometer (AM-MSP series, Analytik & Meßtechnik GmbH, Chemnitz), the specifications of which have been reported elsewhere [14]. Three
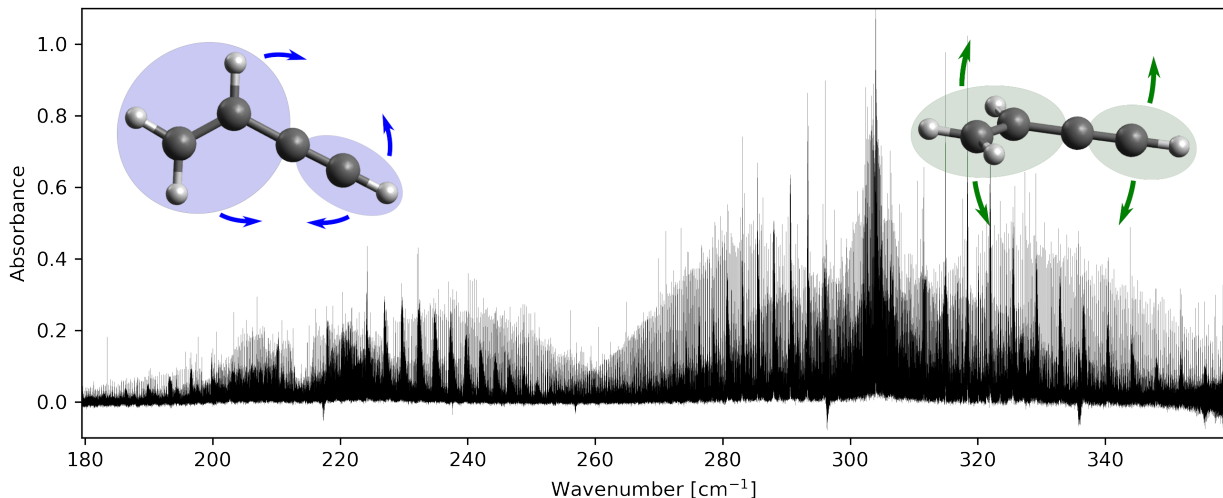
Figure 1: Overview of the FIR vinyl acetylene spectrum recorded at $-83\,°C$ in this work showing the ip bending (ν_{13}, $214\,cm^{-1}$) and oop bending modes (ν_{18}, $304\,cm^{-1}$).
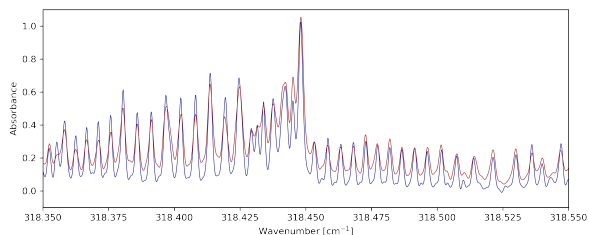

Figure 2: Comparison between the vinylacetylene spectra recorded at $24.8\,°C$ and $2\,mbar$ pressure (red curve) and at $-83\,°C$ and $0.7\,mbar$ (blue curve)

rotational transitions were observed for both the $v_{13} = 1$ and $v_{18} = 1$ states, respectively, $J = 9 - 8$, $J = 10 - 9$, and $J = 13 - 12$ covering $K_a = 0$ up to values as high as 12. Uncertainties of transition frequencies are estimated to be $\leq 15\,kHz$.

3. Quantum-chemical calculations

In the present study, quantum-chemical calculations have been performed at the coupled-cluster singles and doubles (CCSD) level augmented by a perturbative treatment of triple excitations, CCSD(T) [15], together with correlation consistent polarized valence and atomic natural orbital basis sets, i.e. cc-pVXZ, [16] (with X=D and T) and ANOX [17] (with X=0, 1, and 2). The ANO0, ANO1, and ANO2 sets consist of 13s8p6d4f2g to 3s2p1d, 4s3p2d1f, and 5s4p3d2f1fg

contractions for C as well as 8s6p4d3f to 2s1p, 4s2p1d, and 4s3p2d1f contractions for H, respectively. Equilibrium geometries have been calculated using analytic gradient techniques [18], while harmonic frequencies have been computed using analytic second-derivative techniques [19, 20]. For anharmonic computations second-order vibrational perturbation theory (VPT2) [21] has been employed and additional numerical differentiation of analytic second derivatives has been applied to obtain the third and fourth derivatives required for the application of VPT2 [20, 22]. The frozen core approximation has been indicated throughout by "fc". The fc-CCSD(T)/cc-pVTZ force field was done as part of Ref. [10].

All calculations have been carried out using the CFOUR program package [23, 24]; for some of the calculations the parallel version of CFOUR [25] has been used.

4. Analysis and fit

4.1. General considerations - Vibrational level pattern up to $700\,cm^{-1}$

VA is a planar, near-prolate symmetric top molecule with C_s symmetry (Ray's asymmetry parameter $\kappa = -0.98$). Its low-resolution ($0.5\,cm^{-1}$) vibrational spectrum was first described by Tørneng et al. [8]. By symmetry, all of its 18 fundamental modes are IR active and the 13 a'

and 5 a'' fundamental modes show hybrid a/b-type and c-type spectra, respectively. The two lowest fundamental modes, ν_{13} (a') and ν_{18} (a''), are located at 214 cm^{-1} and 304 cm^{-1}, respectively, and are coupled by Coriolis a- and b-type interactions. Whereas the lowest doubly excited state $v_{13} = 2$ is reasonably well separated in energy (see Figure 3 for a schematic representation of the energy levels diagram up to 700 cm^{-1}), the $v_{13} = v_{18} = 1$ combination and $v_{18} = 2$ overtone are close in energy to the next quartet of fundamental modes ($v_{12} = 1$, $v_{17} = 1$ $v_{11} = 1$ and $v_{16} = 1$) and the $v_{13} = 3$ overtone and very likely also coupled by Coriolis and Fermi interactions.
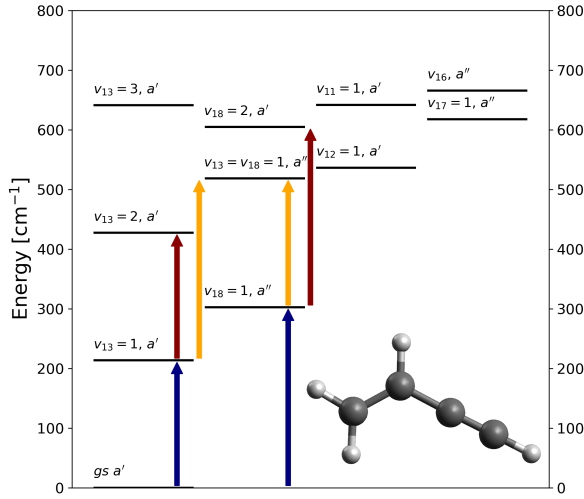

Figure 3: Location and symmetry of the four lowest vibrational fundamentals of vinyl acetylene along with nearby combination and overtone states. Bands studied in this work are indicated by colored arrows.

4.2. Line assignment / ASAP

Spectroscopic analysis of the FIR spectra was performed using the Automated Spectral Line Assignment Procedure (ASAP) described in detail elsewhere (see, e.g., Refs. [26, 27]). In brief, ASAP requires a catalog of predicted transition frequencies observed in the FIR spectra. Uncertainties of state energies within the lower vibrational state (here: vibrational ground state) have to be smaller than the observed FIR linewidths. The procedure selects for any arbitrary rotational level in the upper vibrational state (target state), a group of transitions that share this upper level.

The observed FIR spectrum is recalibrated for each transition by substracting its predicted wavenumber from the wavenumber axis. Thus, all selected transitions peak at the same position in the recalibrated spectra, because deviations between observed and predicted wavenumbers are only due to the uncertainty of the target state. Subsequent multiplication of these recalibrated spectra produces the cross-correlation plot and leads in general to an enhancement of this peak (cross-correlation peak), whereas all other spectral features are surpressed (see Fig. 7 in Ref. [26]). As the cross-correlation peak is located at the difference between observed and calculated transition wavelength, observed transition frequencies or target state energies are finally obtained by adding the determined peak position to their predicted values. In the initial calculation of the cross correlation plots using the ground state rotational data from Ref. [9], it was noticed that $\Delta K = -1, 0, 1$ transitions did not peak exactly at the same wavenumber position on the cross-correlation plots, most likely because the energy difference between the different K-stacks was not accurately determined previously due to the lack of $b-$type transitions in the pure rotational spectrum, which resulted in purely K dependent parameters such as H_K and L_K to be kept fixed in the previous analysis. Nevertheless, the accuracy within each K stack was found here sufficiently accurate to apply ASAP, if each group of transitions included in the calculation of one cross-correlation plot (transitions that have the same upper / target state) was divided into subgroups based on the value of ΔK_a. Consequently cross-correlation plots were calculated separately for each subgroup in the following. In addition, in contrast to previous ASAP applications, transition frequencies (predicted frequency + frequency offset of the cross-correlation peak) rather than state energies were finally used in the fitting procedure. Indeed, most of our previous ASAP investigations focused on the determination of the spectroscopic parameters of excited states, under the assumption that the ground vibrational state was well-described by previous pure rotational and ro-vibrational investigations. As mentioned above, the case of VA is slightly different and an improved characterization of $v = 0$ can be gained also from the analysis of the ro-vibrational spectrum. As a consequence, in this work also the purely K-dependent parameters of the ground vibrational state, such as H_K and L_K that were fixed in the previous analysis [9], could

be released in the fitting procedure. Also, the far better resolved spectrum revealed a different assignment of the Q-branches of ν_{13} compared to Ref. [8] (see below).

At the beginning of fitting, rovibrational transitions of the ν_{13} and ν_{18} fundamentals were included in the analysis along with all millimeter-wave vibrational satellites of these two states (this work, [7]). Subsequently, hot band rovibrational transitions $(2\nu_{13}-\nu_{13}, 2\nu_{18}-\nu_{18}, \nu_{13}+\nu_{18}-\nu_{13}, \nu_{13}+\nu_{18}-\nu_{18})$ were also identified and assigned via ASAP using iteratively updated parameter sets without the need to differentiate between different ΔK_a-subgroups. For consistency, also for these bands, transition frequencies rather than the usual state energies were included in the fit. An uncertainty of $5 \cdot 10^{-4}$ cm^{-1} has been assigned to all rovibrational transition frequencies determined via ASAP.

4.3. Fit

All rovibrational transitions and pure rotational transitions, both from this work and previously published ones [7, 9], were included in the combined dataset. Line fitting was carried out using Pickett's CALPGM suite [28] and a Watson-type Hamiltonian in S-reduction (I^r representation). In total, 25218 rovibrational transitions and 418 pure rotational transitions were included in the combined fit accessing J and K_a values as high as 73 and 19, respectively, for the two lowest vibrationally excited states. The intensity cutoff applied in ASAP for including a line was generally about $\log 10(I/\text{nm}^2\text{MHz}) = -5$. An overview of the datasets is shown in Tab. 1. The parameter set for the vibrational ground state (see Tab. 2) comprises exactly the same parameters as applied in Thorwirth et al. [9], but in the present fit, the parameters H_K and L_K were not kept fixed but released as well. Ground state parameters were also applied to all excited states and difference values, such as ΔA, ΔB, ΔC, etc. were included for the individual excited states (Tab. 3). State energies and interaction parameters are summarized in Tabs. 4 and 5, respectively. As pointed out earlier [7, 8], several of the low-lying vibrational states are coupled by Coriolis and Fermi interactions (see Fig. 3). In the scope of this work, Coriolis a- and b-type interactions between $v_{13} = 1$ and $v_{18} = 1$, between $v_{13} = v_{18} = 1$ and $v_{12} = 1$ as well as between $v_{18} = 2$ and $v_{17} = 1$ were treated. Interactions with ν_{17} and ν_{12} were also explicitly included into the fit, although no spectroscopic data other than their band centers

and the parameters $A-(B+C)$ and D_K of ν_{12} have been derived from experiment so far [8]. First order interaction terms with their associated constants G_a and G_b turned out to be sufficient to reproduce the experimental dataset. Nevertheless, the $G_{a,K}$ term that couples $v_{13} = v_{18} = 1$ with $v_{12} = 1$ has been included, which allowed to omit the parameter ΔH_K for the $v_{13} = v_{18} = 1$ state, whose value exceeded the ground state value H_K otherwise. In general, only parameters that led to an improvement of the fit were released. Otherwise their value was fixed to the corresponding value obtained for the vibrational ground state ($\Delta x = 0$). The combined fit reproduces the dataset to almost experimental accuracy (weighted $rms = 1.03$). Only 39 rovibrational transitions of the hot band $2\nu_{18} - \nu_{18}$ are not well reproduced by the fit ($10 \leq \sigma \leq 15$) and a weighted $rms = 0.92$ is obtained if they are excluded from the fit (see Tab. 1).

Compared to Thorwirth et al. [9], the ground state parameters changed only very slightly. It may be worth mentioning that parameters obtained from CCSD(T) calculations, listed in Tab. 2 as well, are in very good agreement with the experimental ground state values (rotational as well as quartic and sextic centrifugal distortion constants).

A and B rotational constants derived in the combined fit have been corrected for comparison with calculated values and values reported by Tørneng et al. [8] in order to remove contributions from the first order interaction terms that contain the parameters G_a and G_b. The corrected values A^c and B^c are obtained as outlined in previous works [8, 29]

$$A^c = A - \left(\frac{G_a^2}{\Delta E} - (A-C)\frac{G_b^2}{\Delta E^2} + \frac{G_a^2 G_b^2}{\Delta E^2(A-B)} \right) \tag{1}$$

$$B^c = B - \left(\frac{G_b^2}{\Delta E} - (B-C)\frac{G_a^2}{\Delta E^2} - \frac{G_a^2 G_b^2}{\Delta E^2(A-B)} \right) \tag{2}$$

Here, A, B, C, G_a, and G_b are the rotational constants and Coriolis constants as obtained from the fit, and $\Delta E = E(v_1) - E(v_2)$ is the energy difference between the coupled levels. The $A-(B+C)/2$ values 1.490583(57) cm^{-1} and 1.572834(57) cm^{-1} obtained for $v_{13} = 1$ and $v_{18} = 1$ agree within the reported uncertainties with values from Tørneng et al. [8] derived from the microwave measurements. Also the band center determined for ν_{18} is in good agreement between both works, whereas the one ob-
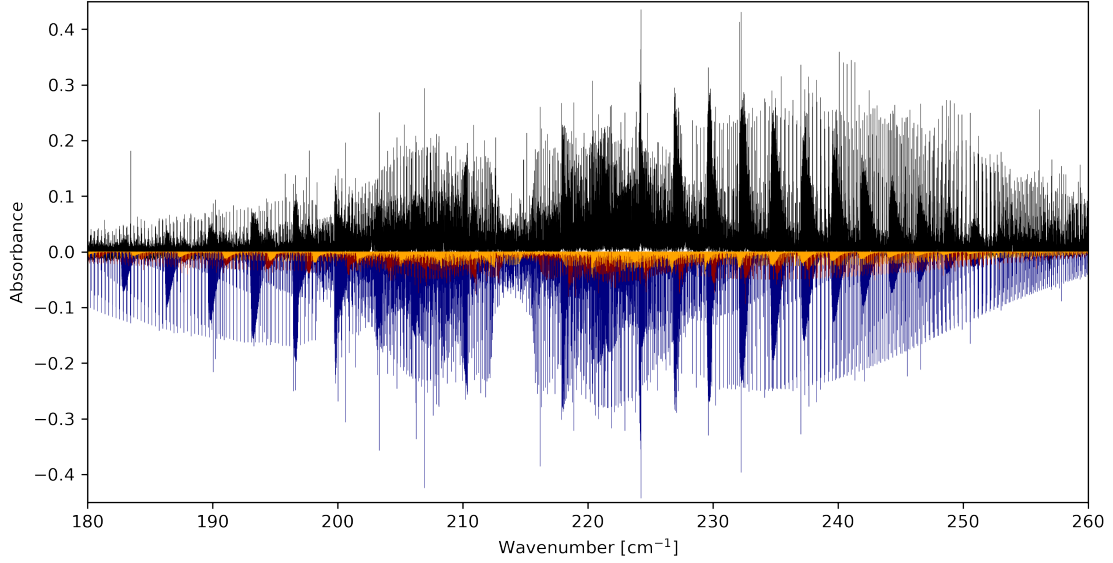
Figure 4: Experimental (post-processed, 0.7 mbar) and calculated spectrum (final set of parameters, this work, $-83\,°\mathrm{C}$) of the fundamental ν_{13} mode. The simulation is obtained by convolution of the predicted transitions (SPCAT) with a FWHM=$0.0016\,\mathrm{cm}^{-1}$ Gaussian profile. The fundamental mode ν_{13} is shown in blue, and the hot bands $2\nu_{13} - \nu_{13}$ and $\nu_{13} + \nu_{18} - \nu_{18}$ in red and orange color, respectively.

Figure 5: Zoom into the experimental and calculated spectrum (final set of parameters, $-83\,°\mathrm{C}$) of the fundamental ν_{13} mode. The simulation is obtained by convolution of the predicted transitions (SPCAT) with a FWHM=$0.0016\,\mathrm{cm}^{-1}$ Gaussian profile. The fundamental mode ν_{13} is shown in blue, and the hot bands $2\nu_{13} - \nu_{13}$ and $\nu_{13} + \nu_{18} - \nu_{18}$ in red and orange color, respectively.
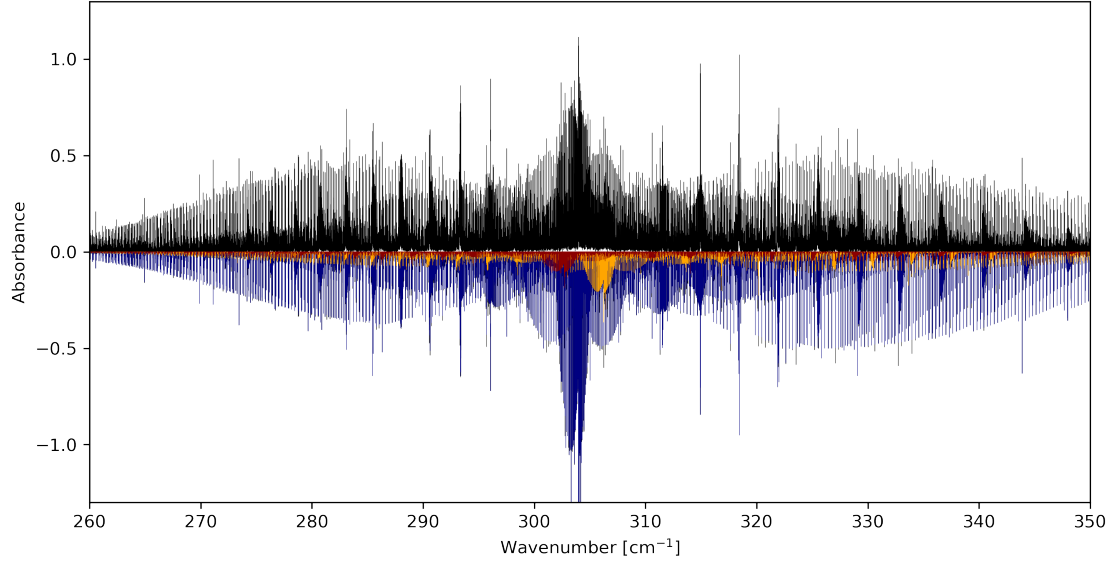
Figure 6: Experimental and calculated spectrum (final set of parameters, $-83\,°\text{C}$) of the fundamental ν_{18} mode. The simulation is obtained by convolution of the predicted transitions (SPCAT) with a FWHM=$0.0016\,\text{cm}^{-1}$ Gaussian profile. The fundamental mode ν_{18} is shown in blue, and the hot bands $2\nu_{18} - \nu_{18}$ and $\nu_{13} + \nu_{18} - \nu_{13}$ in red and orange color, respectively.
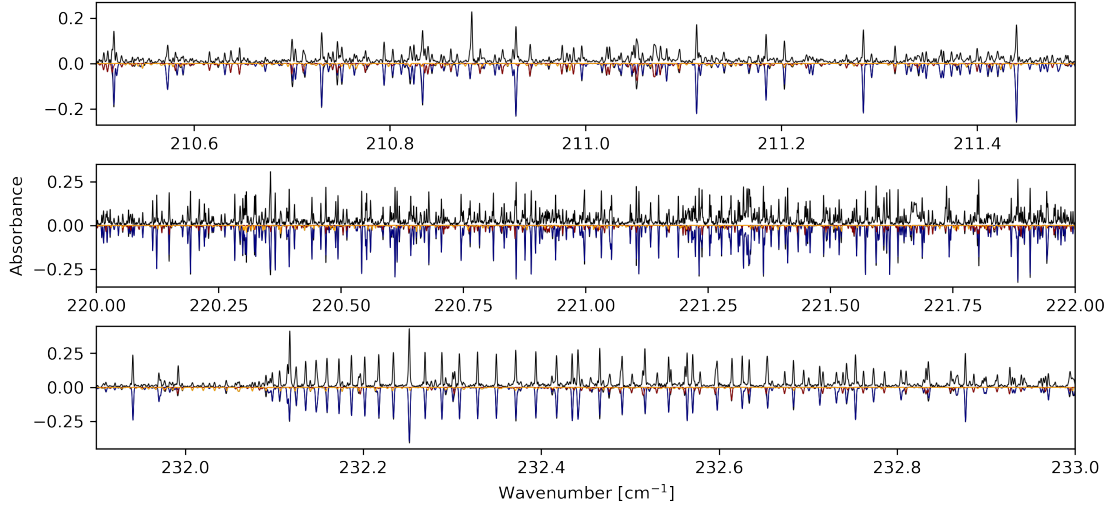

Figure 7: Zoom into the experimental and calculated spectrum (final set of parameters, $-83\,°\text{C}$) of the fundamental ν_{18} mode. The simulation is obtained by convolution of the predicted transitions (SPCAT) with a FWHM=$0.0016\,\text{cm}^{-1}$ Gaussian profile. The fundamental mode ν_{18} is shown in blue, and the hot bands $2\nu_{18} - \nu_{18}$ and $\nu_{13} + \nu_{18} - \nu_{13}$ in red and orange color, respectively.
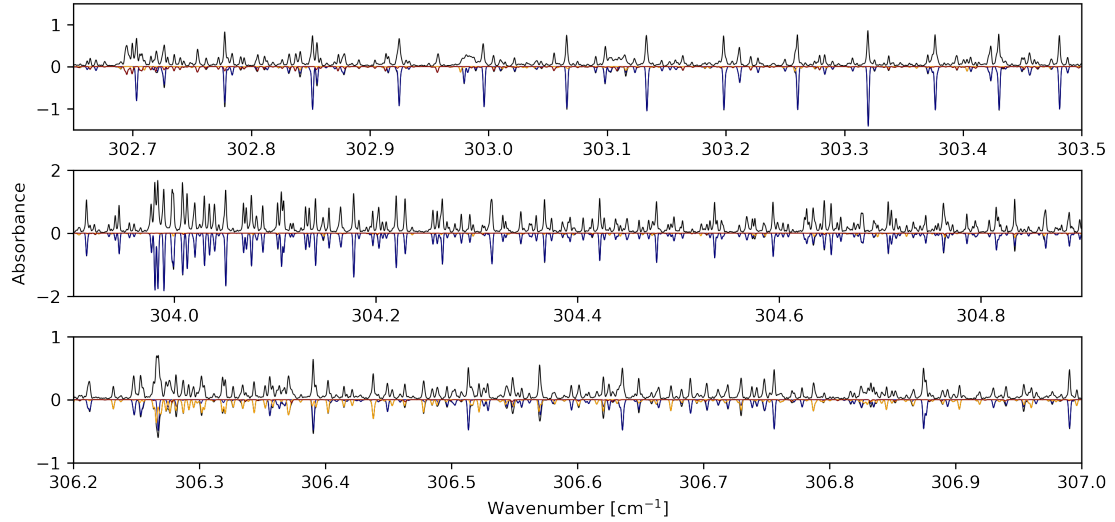
7

Table 1: Experimental datasets.

Microwave	lines	RMS	w. RMS	J_{max}	$K_{a,\,max}$	f_{min}	f_{max}
$v = 0$	289	0.021	0.84	87	23	9	789
$v_{13} = 1$	55	0.026	0.68	13	12	9	119
$v_{18} = 1$	55	0.018	1.23	13	12	9	119
$v_{18} = 2$	4	0.563	1.88	3	1	17	28
$v_{13} = v_{18} = 1$	6	0.503	5.04	3	1	9	28
$v_{13} = 2$	9	0.437	5.17	3	2	9	28
total:	418	0.106	1.31				

Infrared	lines	RMS	w. RMS	J_{max}	$K_{a,\,max}$	f_{min}	f_{max}
ν_{13}	7673	0.299	0.60	73	18	180	271
ν_{18}	6420	0.268	0.54	66	19	250	359
$2\nu_{13} - \nu_{13}$	3753	0.329	0.66	51	9	180	248
$2\nu_{18} - \nu_{18}$	3345	1.188	2.38	53	11	263	349
$\nu_{13} + \nu_{18} - \nu_{13}$	3485	0.290	0.58	54	13	265	356
$\nu_{13} + \nu_{18} - \nu_{18}$	542	0.236	0.47	51	7	195	232
total:	25218	0.51(15.3)	1.02				

Note. Microwave RMS in MHz, Infrared RMS in 10^{-3} cm^{-1} and MHz in brackets, weighted RMS (w. RMS) unitless. Frequency in GHz and cm^{-1}, respectively.

Table 2: Molecular parameters of VA for the vibrational ground state (in MHz).

Parameter		Exp.(this work)	Exp.(Ref. [9])	CCSD(T) [a]
A		50 299.894(26)	50 300.079(36)	50 329.2
B		4744.942 788(68)	4744.942 786(57)	4743.57
C		4329.773 250(61)	4329.773 224(52)	4328.88
D_J	$\times 10^3$	1.822 865(40)	1.822 838(35)	1.800 09
D_{JK}	$\times 10^3$	$-83.2481(14)$	$-83.2492(12)$	-83.2839
D_K	$\times 10^3$	3173.47(41)	3181(2)	3126.92
d_1	$\times 10^3$	$-0.386 874(37)$	$-0.386 798(33)$	$-0.377 747$
d_2	$\times 10^3$	$-0.026 928(12)$	$-0.026 912(13)$	$-0.022 769 4$
H_J	$\times 10^6$	0.004 684 8(85)	0.004 686 7(71)	0.004 74
H_{JK}	$\times 10^6$	$-0.300 03(37)$	$-0.299 74(31)$	$-0.313 302$
H_{KJ}	$\times 10^6$	$-5.920(10)$	$-5.9314(86)$	$-5.940 39$
H_K	$\times 10^6$	408(3)	400	465.076
h_1	$\times 10^9$	1.9087(91)	1.8941(79)	1.8576
h_2	$\times 10^9$	0.2791(14)	0.2757(13)	0.2159
h_3	$\times 10^9$	0.074 89(48)	0.072 38(72)	0.0661
L_J	$\times 10^{12}$	$-0.020 45(54)$	$-0.020 57(45)$	
L_{JJK}	$\times 10^{12}$	1.854(24)	1.832(20)	
L_{JK}	$\times 10^{12}$	$-160(2)$	$-151(2)$	
L_{KKJ}	$\times 10^{12}$	698(18)	692(15)	
L_K	$\times 10^9$	96(6)	-55	
l_1	$\times 10^{15}$	$-10.05(63)$	$-9.13(55)$	

Note. Standard errors are given in parentheses. Parameter is kept fixed in the fit if no error is specified.
[a] A, B, and C rotational constants are calculated from the ae-CCSD(T)/cc-pwCV5Z equilibrium structure [10] and zero-point vibrational corrections obtained at the fc-CCSD(T)/ANO2 level of theory.

Table 3: Molecular parameters of vinyl acetylene in vibrationally excited states derived from the combined fit (in MHz)[a].

Parameter		$v_{13}=1$	$v_{13}=2$	$v_{13}=v_{18}=1$
ΔA		474.0(14)	$-2024.134(60)$	12.97(50)
ΔB		19.543 38(58)	36.3514(37)	20.5356(40)
ΔC		7.476 79(50)	15.2645(33)	17.1405(38)
ΔD_J	$\times 10^3$	0.002 31(11)	0.033 18(80)	0.023 39(93)
ΔD_{JK}	$\times 10^3$	8.0183(59)	20.379(31)	4.54(10)
ΔD_K	$\times 10^3$	$-581.39(62)$	$-1808.87(91)$	$-613(14)$
Δd_1	$\times 10^3$	$-0.008 82(10)$	$-0.015 85(82)$	$-0.005 73(91)$
Δd_2	$\times 10^3$	$-0.009 481(99)$	$-0.002 71(36)$	0.004 18(38)
ΔH_{JK}	$\times 10^6$	0.0947(17)		0.231(30)
ΔH_{KJ}	$\times 10^6$	2.665(34)		13.16(82)

Parameter		$v_{18}=1$	$v_{18}=2$
ΔA		$-141.0(14)$	2960.79(13)
ΔB		2.122 46(58)	5.6287(54)
ΔC		8.597 68(53)	17.7435(49)
ΔD_J	$\times 10^3$	0.007 90(12)	$-0.0145(14)$
ΔD_{JK}	$\times 10^3$	$-6.9604(65)$	$-22.68(11)$
ΔD_K	$\times 10^3$	602.83(56)	2747(3)
Δd_1	$\times 10^3$	0.002 97(16)	0.0103(13)
Δd_2	$\times 10^3$	0.004 23(15)	0.004 28(70)
ΔH_{JK}	$\times 10^6$	$-0.0737(20)$	0.345(42)
ΔH_{KJ}	$\times 10^6$	$-2.808(41)$	$-33.59(86)$
ΔH_K	$\times 10^6$		2840(20)

Parameter	$v_{12}=1$	$v_{17}=1$
ΔA	$-146.7(21)$	$-11 337$
ΔB	$-4.50(14)$	-3.66
ΔC	3.8179	4.51

Note. Standard errors are given in parentheses. Parameter is kept fixed in the fit if no error is specified. Parameters of the ground state are applied to all excited states and difference values are fitted for the individual excited states. Thus, parameters among states and their uncertainty are exactly the same as if no difference parameter was included.
[a] Simultaneous fit to the rotation and rotation-vibration data of the $v=0$, $v_{13}=1,2$, $v_{18}=1,2$, $v_{13}=v_{18}=1$ states.

Table 4: State energies (in cm^{-1}) derived from the combined fit.

State	Symmetry	Energy
$v=0$	a'	0.0^a
$v_{13}=1$	a'	214.010 817(13)
$v_{18}=1$	a''	303.507 507(15)
$v_{13}=2$	a'	428.639 982(30)
$v_{13}=v_{18}=1$	a''	519.823 656(36)
$v_{18}=2$	a''	605.702 465(41)
$v_{12}=1$	a'	539.2212(15)
$v_{17}=1$	a''	621.1042(23)

[a] Fixed.

Table 5: Interaction parameters (in MHz) derived from the combined fit.

State	Parameter	Value
$\nu_{13} \longleftrightarrow \nu_{18}$	G_a	64 213(29)
$\nu_{13} \longleftrightarrow \nu_{18}$	G_b	1580.148 792
$\nu_{13} + \nu_{18} \longleftrightarrow \nu_{12}$	G_a	$-862(146)$
$\nu_{13} + \nu_{18} \longleftrightarrow \nu_{12}$	G_b	473.22(19)
$\nu_{13} + \nu_{18} \longleftrightarrow \nu_{12}$	$G_{a,K}$	23.514(91)
$2\nu_{18} \longleftrightarrow \nu_{17}$	G_a	$-1753.81(71)$

Note. Standard errors are given in parentheses. Parameter is kept fixed in the fit if no error is specified.

Table 6: Comparison of fundamental frequencies and anharmonicity constants (in cm^{-1}) between experiment and ab initio calculation.

Parameter	Calc.	Exp.	Obs.-Calc.	Ref. [8]
ν_{13}	213.5	214.010 817(13)	0.5	217.21(13)
ν_{18}	302.6	303.507 507(15)	0.9	303.56(7)
ν_{12}	536.4	539.2212(15)	2.8	539.21(3)
ν_{17}	617.5	621.1042(23)	3.6	618
$\chi_{13,13}$	0.300	0.309 173(20)	0.009	
$\chi_{18,18}$	-0.671	$-0.656 274(25)$	0.015	
$\chi_{13,18}$	2.290	2.305 332(38)	0.016	

Note. Fundamental frequencies and anharmonicity constants χ are calculated using the fc-CCSD(T)/ANO2 level of theory. Experimental values are derived from state energies determined in the combined fit (Tab. 4).

tained for ν_{13} differs by about 3 cm^{-1}, which is due to a different assignment of the Q-branches that are shifted by one K_a towards lower frequencies in the present work. The agreement between experimental and calculated values is excellent. Band centers match to within 1 cm^{-1} (Tab. 4) and rotational constants within 1–2 ‰ (Tab. 7). Also the Coriolis coupling constants $\zeta^a_{13,18}$ and $\zeta^b_{13,18}$ that are related to the parameters G_a and G_b via

$$\zeta_a = \frac{G_a}{A}\left(\sqrt{\nu_{13}/\nu_{18}} + \sqrt{\nu_{18}/\nu_{13}}\right)^{-1} \quad (3)$$

$$\zeta_b = \frac{G_b}{B}\left(\sqrt{\nu_{13}/\nu_{18}} + \sqrt{\nu_{18}/\nu_{13}}\right)^{-1}, \quad (4)$$

agree well between experiment and calculation. Tab. 8 lists their values along with calculated values using different basis sets. The scatter of calculated values, which is less than 2 % of the reported value, shows only a minor dependence on the applied basis sets. Thus, reliable values are already obtained at rather low computational costs. G_b, and thus ζ_b was fixed in the final version of the combined fit to reduce the number of correlations among parameters without degradation of the fit. If re-

leased, the value $\left|\zeta^b_{13,18}\right|^a = 0.151(10)$ is derived in reasonable agreement with calculations.

The overtone $v_{13} = 2$, next lowest in energy, is comparably isolated and the observations could be reproduced within experimental accuracy without the inclusion of any interactions. Nevertheless, the comparably large values of ΔD_K and ΔH_K might be indicative of the presence of interactions. Clearly, numerous transitions that belong to the combination $\nu_{13} + \nu_{18}$ and to the hot band $2\nu_{18} - \nu_{18}$ are perturbed. Despite the limited spectral information, a-type Coriolis interaction terms that couple $v_{13} = v_{18} = 1$ with $v_{12} = 1$, which is close in energy, are included to reproduce the spectrum of the former. Parameters ΔA, ΔB and the band center of ν_{12} are released and determined from the fit whereas ΔC was kept fixed at the calculated value. Their values $[(\Delta A - (\Delta B + \Delta C)/2 = -141.4(19)$ MHz] are in agreement with [8] $[\Delta A - (\Delta B + \Delta C)/2 = -180(70)$ MHz] and calculations.

The interaction partner of $v_{18} = 2$ is less certain. Here, the observed transitions can either be reproduced by Fermi interactions with $v_{11} = 1$ or by a-type Coriolis interactions with $v_{17} = 1$. Al-

Table 7: Comparison of rotation–vibration interaction constants α (in MHz) between experiment and calculation.

Parameter	$v_{12} = 1$	$v_{13} = 1$	$v_{17} = 1$	$v_{18} = 1$
ΔA^c_{exp}	$-145.4(19)$	$-1062.8(17)$	$-11\,343.66$ [a]	$1395.8(17)$
$-\alpha^A_{calc}$	-146.88	-987.96	$-11\,337.05$	1373.74
ΔB^c_{exp}	$-4.11(11)$	$18.888\,57(51)$	-3.65 [a]	$3.318\,66(56)$
$-\alpha^B_{calc}$	-4.62	18.59	-3.66	2.86
ΔC_{exp}	-3.82 [a]	$7.476\,79(50)$	4.51 [a]	$8.597\,68(53)$
$-\alpha^C_{calc}$	-3.82	7.63	4.51	8.40
	$v_{13} = 2$	$v_{18} = 2$	$v_{13} = v_{18} = 1$	
ΔA^c_{exp}	$-2024.134(60)$	$2967.45(11)$	$11.72(58)$	
ΔA_{calc}	-1975.91	2747.49	385.79	
ΔB^c_{exp}	$36.3514(37)$	$5.6345(49)$	$20.1515(33)$	
ΔB_{calc}	37.17	5.71	21.44	
ΔC_{exp}	$15.2645(33)$	$17.7435(49)$	$17.1405(38)$	
ΔC_{calc}	15.27	16.80	16.04	

Note. Experimental values are taken from the combined fit. $\Delta A = A_v - A_0 = -\alpha^A_i$, same for ΔB and ΔC. The c superscript in ΔA^c and ΔB^c denotes values corrected according to Eqs. (1) and (2) in order to remove contributions from the first order interaction terms. For overtones and combination modes, the ΔA values reported correspond to the sum of the α_i of the involved modes.
[a] fixed in the combined fit.

Table 8: Coriolis coupling constants $\zeta^a_{13;18}$ and $\zeta^b_{13;18}$ (Unitless.)

Parameter	Exp.	fc-CCSD(T)				
		ANO0	ANO1	ANO2	cc-pVDZ	cc-pVTZ
$\left\|\zeta^a_{13,18}\right\|$	$0.628\,68(27)$	0.674	0.665	0.663	0.677	0.667
$\left\|\zeta^b_{13,18}\right\|$	0.164 [a]	0.165	0.165	0.164	0.163	0.163

Note. [a] Parameter G_b was fixed to the fc-CCSD(T)/ANO2 value in the final version of the combined fit (see text). $\left|\zeta^b_{13,18}\right| = 0.151(10)$ is obtained, if G_b is released.

though a better rms was obtained including the former, Coriolis interactions appear a more probable cause, because rotational constants of $v_{11} = 1$ obtained in the former approach are much smaller (e.g., $\Delta A \approx -17\,\text{GHz}$) than the ground state values, which is in contrast to the calculated values that predict large, positive ΔA values for this state. On the other hand, rotational constants of $v_{17} = 1$ can be fixed to the calculated values if coupled with ν_{17}. However, it is expected that a more detailed study of the coupling will reveal also other couplings among the levels besides the one discussed here. Another justification of the validity of the analysis is the excellent match between the anharmonicity constants derived from the fitted parameters and the calculated values as shown in Tab. 6. Finally, transition frequencies and intensities have been calculated with SPCAT based on the current analysis and used to simulate the experimental spectrum at $-83\,°\text{C}$ (Figs. 4 and 6). Close-up views of selected parts of the spectrum are presented in Figs. 5 and 7. The very good agreement between simulation and experiment shows the quality of the predictions and validates also the overall correctness of assignments done with ASAP. Partition functions have been calculated based on the summation of energies. All states investigated in this work ($v = 0$; $v_{13} = 1, 2$; $v_{18} = 1, 2$; $v_{13} = v_{18} = 1$; $v_{12} = 1$; and $v_{17} = 1$) and energy levels up to $J = 120$ and $K_a = 35$ have been taken into account. A listing

of the experimental dataset and partition functions will be given in the supplementary material in electronic form.

5. Conclusions and prospects

The present high-resolution FIR study of VA has provided a greatly extended description of the two energetically lowest vibrational fundamental modes ν_{13} and ν_{18}. In addition, spectroscopic signatures of several hot bands associated with both fundamentals were identified, assigned and fitted under consideration of Coriolis as well as Fermi interactions. Possible influences of other states remaining unstudied (ν_{11}, ν_{17}) on the states studied here in great detail have been considered through explicit perturbation treatment. However, the limited data situation in many energetically low-lying states calls for an extension of the spectroscopic work, either through high-resolution infrared studies of additional vibrational fundamentals (for example ν_{12}, ν_{16}, ν_{17}) and associated hot bands or through a more comprehensive study of the vibrational satellite pattern in pure rotational spectra or possibly even both. While generally feasible, in any case, spectroscopic analyses of such vibrational polyads will be challenging due to the presence of numerous perturbations. It might even be useful to further extend the ground state pure rotational spectrum of VA. Provided sufficiently high quantum numbers are reached such a study might also yield insight into a conceivable interaction of the ground state with the ν_{13} mode (see, e.g., Ref. [30] for a similar situation in isoelectronic acrylonitrile).

The present study is yet another manifestation of the usefulness of the Automated Spectral Line Assignment Procedure (ASAP) towards convenient data reduction of high-resolution infrared data.

After submission of this work, Cernicharo et al. finally reported on the radio astronomical detection of VA in the prototypical dark cloud TMC-1 [31].

Acknowledgement

Appendix: Supplementary data

Supplementary data associated with this article (parameter and fit files) are available on ScienceDirect (www.sciencedirect.com).

References

[1] J. Cernicharo, The Polymerization of Acetylene, Hydrogen Cyanide, and Carbon Chains in the Neutral Layers of Carbon-rich Proto-planetary Nebulae, Astrophys. J. 608 (2004) L41–L44. doi:10.1086/422170.

[2] Y. S. Kim, R. I. Kaiser, An infrared spectroscopic study of amorphous and crystalline ices of vinylacetylene and implications for Saturn's satellite Titan, Astron. Astrophys. Suppl. Ser. 181 (2009) 543–547. doi:10.1088/0067-0049/181/2/543.

[3] G. A. Sobolev, A. M. Shcherbakov, P. A. Akishin, Rotational spectrum and the dipole moment of the vinylacetylene molecule, Opt. Spectrosc. 12 (1962) 147.

[4] S. Thorwirth, H. Lichau, The millimeter-wave spectrum and the dipole moment of vinylacetylene, Astron. Astrophys. 398 (2003) L11–L13. doi:10.1051/0004-6361:20021849.

[5] G. Tasi, M. Szöri, A. G. Császár, Semispectroscopic and quantitative structure - Property relationship estimates of the equilibrium and vibrationally averaged structure and dipole moment of 1-buten-3-yne, J. Phys. Chem. A 109 (2005) 4824–4828. doi:10.1021/jp058005b.

[6] H. W. Morgan, J. H. Goldstein, The Microwave Spectrum of Vinylacetylene, J. Chem. Phys. 20 (1952) 1981. doi:10.1063/1.1700372.

[7] C. Hirose, Microwave Spectra of Vinylacetylene and Monodeutero Vinylacetylene in Ground and Excited Vibrational States, Bull. Chem. Soc. Japan 43 (1970) 3695–3698. doi:10.1246/bcsj.43.3695.

[8] E. Tørneng, C. J. Nielsen, P. Klaboe, H. Hopf, H. Priebe, The IR, Raman and Microwave-Spectra of 1-butene-3-yne (Vinylacetylene) and 1-butene-3-yne-4D, Spectrochim. Acta A36 (1980) 975–987. doi:10.1016/0584-8539(80)80177-2.

[9] S. Thorwirth, H. S. P. Müller, H. Lichau, G. Winnewisser, G. C. Mellau, The submillimeter wave spectrum of the C_4H_4 isomer vinylacetylene, J. Mol. Struct. 695 (2004) 263–267. doi:10.1016/j.molstruc.2004.01.002.

[10] S. Thorwirth, M. E. Harding, J. B. Dudek, M. C. McCarthy, Equilibrium molecular structures of vinyl carbon chains: Vinyl acetylene, vinyl diacetylene, and vinyl cyanide, J. Mol. Spectrosc. 350 (2018) 10–17. doi:10.1016/j.jms.2018.05.001.

[11] C.-H. Chang, D. J. Nesbitt, Sub-Doppler infrared spectroscopy of propargyl radical (H_2CCCH) in a slit supersonic expansion, J. Chem. Phys. 142 (2015) 244313. doi:10.1063/1.4922931.

[12] R. Schermaul, J. W. G. Seibert, G. C. Mellau, M. Winnewisser, Variable-temperature 3-m absorption cell developed for spectroscopic measurements of gases, Applied Optics 35 (1996) 2884–2890. doi:10.1364/ao.35.002884.

[13] V.-M. Horneman, R. Anttila, S. Alanko, J. Pietilä, Transferring calibration from CO_2 laser lines to far infrared water lines with the aid of the ν_2 band of OCS and the ν_2, $\nu_1 - \nu_2$, and $\nu_1 + \nu_2$ bands of $^{13}CS_2$: Molecular constants of $^{13}CS_2$, Journal of Molecular Spectroscopy 234 (2005) 238–254. doi:10.1016/j.jms.2005.09.011.

[14] M. Winnewisser, H. Lichau, F. Wolf, The Rotational Spectrum of OCCCS Revisited, J. Mol. Spectrosc. 202 (2000) 155–162. doi:10.1006/jmsp.2000.8131.

[15] K. Raghavachari, G. W. Trucks, J. A. Pople, M. Head-Gordon, A 5th-order perturbation comparison of electron correlation theories, Chem. Phys. Lett. 157 (1989) 479–483. doi:10.1016/S0009-2614(89)87395-6.

[16] T. H. Dunning, Gaussian basis sets for use in correlated molecular calculations .1. The atoms boron through neon and hydrogen, J. Chem. Phys. 90 (1989) 1007–1023. doi:10.1063/1.456153.

[17] J. Almlöf, P. R. Taylor, General contraction of Gaussian basis sets .1. Atomic natural orbitals for 1st-row and 2nd-row atoms, J. Chem. Phys. 86 (1987) 4070–4077. doi:10.1063/1.451917.

[18] J. D. Watts, J. Gauss, R. J. Bartlett, Open-shell analytical energy gradients for triple excitation many-body, coupled-cluster methods - MBPT(4), CCSD+T(CCSD), CCSD(T), and QCISD(T), Chem. Phys. Lett. 200 (1992) 1–7. doi:10.1016/0009-2614(92)87036-0.

[19] J. Gauss, J. F. Stanton, Analytic CCSD(T) second derivatives, Chem. Phys. Lett. 276 (1997) 70–77. doi:10.1016/S0009-2614(97)88036-0.

[20] J. F. Stanton, J. Gauss, Analytic second derivatives in high-order many-body perturbation and coupled-cluster theories: computational considerations and applications, Int. Rev. Phys. Chem. 19 (2000) 61–95. doi:10.1080/014423500229864.

[21] I. M. Mills, Vibration-Rotation Structure in Asymmetric- and Symmetric-Top Molecules, Academic Press, New York, 1972, pp. 115–140.

[22] J. F. Stanton, C. L. Lopreore, J. Gauss, The equilibrium structure and fundamental vibrational frequencies of dioxirane, J. Chem. Phys. 108 (1998) 7190–7196. doi:10.1063/1.476136.

[23] J. F. Stanton, J. Gauss, L. Cheng, M. E. Harding, D. A. Matthews, P. G. Szalay, CFOUR, Coupled-Cluster techniques for Computational Chemistry, a quantum-chemical program package, . With contributions from A.A. Auer, R.J. Bartlett, U. Benedikt, C. Berger, D.E. Bernholdt, Y.J. Bomble, O. Christiansen, F. Engel, R. Faber, M. Heckert, O. Heun, M. Hilgenberg, C. Huber, T.-C. Jagau, D. Jonsson, J. Jusélius, T. Kirsch, K. Klein, W.J. Lauderdale, F. Lipparini, T. Metzroth, L.A. Mück, D.P. O'Neill, D.R. Price, E. Prochnow, C. Puzzarini, K. Ruud, F. Schiffmann, W. Schwalbach, C. Simmons, S. Stopkowicz, A. Tajti, J. Vázquez, F. Wang, J.D. Watts and the integral packages MOLECULE (J. Almlöf and P.R. Taylor), PROPS (P.R. Taylor), ABACUS (T. Helgaker, H.J. Aa. Jensen, P. Jørgensen, and J. Olsen), and ECP routines by A. V. Mitin and C. van Wüllen. For the current version, see http://www.cfour.de.

[24] D. A. Matthews, L. Cheng, M. E. Harding, F. Lipparini, S. Stopkowicz, T.-C. Jagau, P. G. Szalay, J. Gauss, J. F. Stanton, Coupled-cluster techniques for computational chemistry: The CFOUR program package, J. Chem. Phys. 152 (2020) 214108. doi:10.1063/5.0004837.

[25] M. E. Harding, T. Metzroth, J. Gauss, A. A. Auer, Parallel calculation of CCSD and CCSD(T) analytic first and second derivatives, J. Chem. Theory Comput. 4 (2008) 64–74. doi:10.1021/ct700152c.

[26] M. A. Martin-Drumel, C. P. Endres, O. Zingsheim, T. Salomon, J. van Wijngaarden, O. Pirali, S. Gruet, F. Lewen, S. Schlemmer, M. C. McCarthy, S. Thorwirth, The SOLEIL view on sulfur rich oxides: The S_2O bending mode ν_2 at 380 cm^{-1} and its analysis using an Automated Spectral Assignment Procedure (ASAP), J. Mol. Spectrosc. 315 (2015) 72–79. doi:10.1016/j.jms.2015.02.014.

[27] C. P. Endres, M.-A. Martin-Drumel, O. Zingsheim, L. Bonah, O. Pirali, T. Zhang, Á. Sánchez-Monge, T. Möller, N. Wehres, P. Schilke, et al., SOLEIL and ALMA views on prototypical organic nitriles: C_2H_5CN, Journal of Molecular Spectroscopy 375 (2021) 111392. doi:10.1016/j.jms.2020.111392.

[28] H. M. Pickett, The fitting and prediction of vibration-rotation spectra with spin interactions, J. Mol. Spectrosc. 148 (1991) 371–377. doi:10.1016/0022-2852(91)90393-0.

[29] I. Mills, Coriolis interactions, intensity perturbations and potential functions in polyatomic molecules, Pure Appl. Chem. 11 (1965) 325–344. doi:10.1351/pac196511030325.

[30] Z. Kisiel, M.-A. Martin-Drumel, O. Pirali, Lowest vibrational states of acrylonitrile from microwave and synchrotron radiation spectra, J. Mol. Spectrosc. 315 (2015) 83 – 91. doi:10.1016/j.jms.2015.03.003.

[31] J. Cernicharo, M. Agúndez, C. Cabezas, N. Marcelino, B. Tercero, J. R. Pardo, J. D. Gallego, F. Tercero, J. A. López-Pérez, P. de Vicente, Discovery of CH_2CHCCH and detection of HCCN, HC_4N, CH_3CH_2CN, and, tentatively, CH_3CH_2CCH in TMC-1, Astron. Astrophys. 647 (2021) L2. doi:10.1051/0004-6361/202140434.